BJR|Open https://doi.org/10.1259/bjro.20190001

Received: 26 December 2018 | Revised: 23 February 2019 | Accepted: 29 March 2019

Cite this article as:
Gabelloni M, Faggioni L, Neri E. Imaging biomarkers in upper gastrointestinal cancers. *BJR Open* 2019; **1**: 20190001.

REVIEW ARTICLE

# Imaging biomarkers in upper gastrointestinal cancers

**MICHELA GABELLONI, MD, MSc, LORENZO FAGGIONI, MD, PhD and EMANUELE NERI, MD**

Department of Translational Research, Diagnostic and Interventional Radiology, University of Pisa, Pisa, Italy

Address correspondence to: Dr Michela Gabelloni
E-mail: *mgabelloni@sirm.org*

**ABSTRACT**

In parallel with the increasingly widespread availability of high performance imaging platforms and recent progresses in pathobiological characterisation and treatment of gastrointestinal malignancies, imaging biomarkers have become a major research topic due to their potential to provide additional quantitative information to conventional imaging modalities that can improve accuracy at staging and follow-up, predict outcome, and guide treatment planning in an individualised manner. The aim of this review is to briefly examine the status of current knowledge about imaging biomarkers in the field of upper gastrointestinal cancers, highlighting their potential applications and future perspectives in patient management from diagnosis onwards.

## INTRODUCTION

The term "biomarker" refers to a characteristic that is objectively measured and evaluated as an indicator of normal biologic processes, pathogenic processes, or biological responses to therapeutic interventions.[1–3] Biomarkers can be derived directly from human biological samples (including blood or other biological fluids, tissues or cells) or biosignals detected by diagnostic imaging techniques (such as multidetector CT, MRI, ultrasound or PET), providing anatomical and/or functional parameters that correlate with histopathological or molecular data.[4–7] Imaging biomarkers can be either quantitative (*e.g.* lesion diameter or volume, CT density, MR signal intensity, radiomics features, and any other biomarker whose magnitude can be expressed as a quantity value) or qualitative (*e.g.* pathological grading systems that can be expressed as ordinal rather than continuous quantitative data, such as clinical TNM staging, BI-RADS, LI-RADS, PI-RADS, C-RADS, and so on).[8,9] Compared to "real" biological samples, imaging biomarkers have the advantage of being noninvasive (or minimally invasive) and easily obtainable, making them attractive for repeated testing and follow-up. In addition, while conventional biopsy captures only a fraction of tumour cells that may not be representative of the entire tumour, imaging biomarkers can capture the whole tumour heterogeneity, thus playing a potentially critical role into guiding biopsy or whenever biopsy is unobtainable.[10–12]

Due to the incremental diagnostic and prognostic value that imaging biomarkers can provide over conventional modalities (which, however, remain indispensable for the routine diagnostic workup of cancer patients), a great interest has arisen in the scientific and medical community in searching for biomarkers and building biobanks that may lead to more effective, patient-specific treatment. In this perspective, extensive research has recently been made in the field of radiomics, a discipline dealing with high-throughput extraction and analysis of quantitative features from diagnostic images that cannot usually be derived from visual assessment (including shape/size-, histogram- or filter-based texture analysis) and form the quantitative imaging expression of pathological processes that are also expressed by other "omics", such as genomics, transcriptomics, metabolomics and proteomics.[5,8]

In this paper we will give a brief, yet hopefully explanatory overview of the current potential role of imaging biomarkers in the management of upper gastrointestinal cancers, with oropharyngeal, oesophageal, and gastric cancers as paradigm diseases.

## OROPHARYNGEAL CANCER

Head and neck cancer is the seventh most frequent cancer and the ninth most frequent cause of cancer-related death, with a worldwide incidence of 550,000 cases and 380,000 deaths annually, of which 90% are squamous cell carcinomas (SCC) in the adult population.[13,14] Most oropharyngeal cancers are diagnosed at a locally advanced stage, usually requiring multimodality treatment (including surgery, chemotherapy and/or radiation therapy), and the rate of locoregional recurrence is as high as 25–50% depending on the lesion site, making recurrence risk the

greatest hurdle in improving survival rate. Moreover, tumour biology (with particular reference to human papillomavirus [HPV] positivity) plays a pivotal role in defining the prognosis and optimal therapeutic strategy for patients with head and neck SCC, with HPV+oropharyngeal SCC being associated with a better overall survival. Therefore, a comprehensive assessment of disease extension (including primary tumour site and locoregional lymph nodes) at baseline and after treatment is mandatory, also in consideration that oropharyngeal and other head and neck SCC recurrences tend to occur at a locoregional level within the same volume of treatment.[15–17]

Although conventional multidetector CT and MR imaging performed with state-of-the-art equipment is the mainstay for diagnosis, staging and follow-up of patients with oropharyngeal SCC, morphologic imaging can be limited in detecting subtle disease or differentiating disease recurrence from benign post-treatment changes (*e.g.* after surgery and/or radiation therapy) that may obscure viable tumour tissue or mimic disease, and usually cannot provide *per se* any insight about prognosis, likelihood of early and/or sustained treatment response, or eligibility to patient-tailored target therapies.[14,18–20] On the other hand, both standard CT and MRI data and those derived from more complex implementations of cross-sectional imaging can be joined to build specific radiomic signatures that can lead to improved patient stratification and potentially more personalised treatment[8,21] (Table 1). In this latter setting, a recent large multicentre study by Leijenaar et al combining 902 radiomic features from 778 patients with oropharyngeal SCC showed that CT-based radiomics can predict HPV+ (p16) status from multivariable models obtained from standard pre-treatment CT images. More specifically, a model was developed on all training data ($M_{all}$) and on an artefact-free subset of training data ($M_{no\ art}$) to assess the impact of CT artefacts in predicting HPV (p16), and a consistent and significant split was observed between survival curves with HPV status determined by p16 [$p = 0.007$, hazard ratio (HR) 0.46], $M_{all}$ ($p = 0.036$, HR 0.55) and $M_{no\ art}$ ($p = 0.027$, HR 0.49), along with an area under the receiver operator curve ranging between 0.70 and 0.80 for both $M_{all}$ and $M_{no\ art}$.[22] In addition, evidence is growing that a radiomic approach can provide useful prognostic quantitative information in patients undergoing chemo-radiation therapy (CRT), such as primary tumour volume (which correlates with treatment outcome better than T or N stages),[23] CT texture analysis (which can predict local failure after CRT),[24] and $^{18}$F-FDG PET texture as a predictor of post-CRT patient survival in addition to clinical variables.[25]

Among MRI techniques, diffusion-weighted imaging (DWI) is a powerful quantitative biomarker that can identify foci of residual disease as areas of restricted diffusivity of water molecules, due to cancer cells being densely packed with a relatively high nuclear-cytoplasmic ratio compared with non-neoplastic tissues. This allows overcoming potential confounding factors such as diffuse oedema and contrast enhancement as a result of inflammation and/or post-radiation sequelae, or faint or no enhancement in poorly vascularised and/or highly necrotic tumours, resulting in increased sensitivity in detection of primary oropharyngeal SCC.[14,20] In a recent large meta-analysis, DWI-based apparent diffusion coefficient (ADC) quantitative assessment outperformed anatomical MRI for detection of primary tumour site with a pooled sensitivity and specificity of 89% and 86% *vs* 84% and 82%, respectively.[20] Lower ADC values have also been found in malignant than in benign lymph nodes sized down to 5–10 mm, and Holzapfel et al were able to correctly classify cervical lymph nodes as benign or malignant using an ADC threshold of $1.02 \times 10^{-3}$ mm$^2$/s in 94.3% of cases.[14,26,27] Furthermore, Hwang et al assessed the performance of standard ($b = 1000$ s/mm$^2$) and high b-value (2000 s/mm$^2$) DWI in differentiating between recurrent tumour and post-treatment changes, and found that the ratio between $ADC_{2000}$ and $ADC_{1000}$ was significantly higher in the former than in the latter (73.5% *vs* 56.9%, $p < 0.001$), with a cut-off value of 62.6% leading to a sensitivity, specificity, and diagnostic accuracy of 95.0%, 69.2%, and 84.8%, respectively.[28] Of interest, patients with a good response to induction neoadjuvant chemotherapy were found to have lower $ADC_{2000}$ values along with smaller tumour volume than poor responders, suggesting a potential role of high ADC values in predicting tumour response.[29] In terms of risk stratification, it has been reported that the combination of poor prognostic factors such as high $^{8}$F-FDG PET-CT-derived $SUV_{maxT/B}$ and high $ADC_{min}$ values improves the prognostic role of the two separate parameters (with high $ADC_{min}$ identifying SCC patients with worse prognosis among those with high $SUV_{maxT/B}$).[30] Moreover, a significant association was observed between histopathological markers of tumour proliferation and ADC and SUV values calculated at simultaneous $^{18}$F-FDG-PET/MRI, with mean ADC being negatively correlated with Ki67 level ($r = -0.728$, $p = 0.011$) and total nucleic area ($r = -0.691$, $p = 0.019$), and combined $SUV_{max}/ADC_{min}$ positively correlated with average nucleic area ($r = 0.627$, $p = 0.039$).[31]

Other functional imaging modalities such as dynamic contrast enhancement (DCE)-MRI, CT perfusion imaging and dual energy CT (DECT) can enable a quantitative evaluation of tumour vascularity that can be useful in the pre- and post-treatment setting.[14,32] In general, highly vascular SCC tend to have a better treatment response compared to less vascular ones due to their greater sensitivity to radiation and better delivery of chemotherapeutic drugs, yet they may have poorer outcome due to a higher metastatic potential.[14,33] In terms of grading, quantitative DCE-MRI parameters such as the blood volume transfer constant ($K_{trans}$), the extracellular volume fraction ($V_e$), and the initial area under the curve (iAUC) were shown to be higher in poorly than in well-differentiated SCC, with $K_{trans}$ having the greatest diagnostic significance at a cut-off value of 0.270 min$^{-1}$ and an overall diagnostic sensitivity and specificity of 95.0 and 90.9%.[34] Chen et al found that DCE-MRI parameters [$K_{trans}$, $V_e$ and the rate constant of contrast transfer ($K_{ep}$)] allowed to discriminate among tumour, metastatic lymph nodes and normal tissue, with $K_{trans}$ and $V_e$ values of normal tissue being significantly lower from those of nodes ($p < 0.001$) and primary tumours ($p < 0.001$), whereas $K_{ep}$ values of primary tumours were significantly higher from those of nodes ($p = 0.001$) and normal tissue ($p = 0.002$), respectively.[35] Moreover, Baker et al reported that DCE-MRI can predict tumour response to target therapies with EGFR-targeted tyrosine kinase inhibitors, in conjunction with $^{18}$F-FDG PET.[36]

Table 1. Summary of the features and main findings of the studies on imaging biomarkers in head and neck cancer (with particular reference to oropharyngeal cancer) cited in the text. Case reports and general reviews articles are not included. References are sorted in the order in which they appear in the text

| Reference | Tumour type and location | Imaging features | Endpoints | Main findings |
|---|---|---|---|---|
| van der Hoorn et al.[20] | Head and neck SCC (oral cavity, pharynx, larynx)[a] | Anatomical MRI, ADC | Diagnostic accuracy for treatment response evaluation | • Pooled analysis of anatomical MRI of the primary site showed a sensitivity of 84% (95% confidence interval 72÷92%) and specificity of 82% (71÷89%)<br>• ADC of the primary site showed a pooled sensitivity of 89% (74÷96%) and specificity of 86% (69÷94%) |
| Leijenaar et al.[22] | HPV+ oropharyngeal SCC | Radiomic signatures ($M_{all}$, $M_{no\ art}$) for HPV (p16) prediction from standard pre-RT/CRT CT imaging | Diagnostic accuracy, OS | • AUC for $M_{all}$ and $M_{no\ art}$ as high as 0.70÷0.80<br>• Consistent and significant split between survival curves with HPV status determined by p16 ($p = 0.007$, HR 0.46), $M_{all}$ ($p = 0.036$, HR 0.55) and $M_{no\ art}$ ($p = 0.027$, HR 0.49) |
| Strongin et al.[23] | Locally advanced SCC (oropharynx, hypopharynx and larynx) | Primary tumour volume (TV) before CRT | PFS, OS | • Better 5-year prognosis with primary TV <35 $cm^3$ (71% *vs* 43%, $p = 0.01$)<br>• Longer PFS and OS with primary TV <35 $cm^3$ (61% *vs* 33%, $p = 0.022$ and 84 *vs* 41%, $p < 0.001$, respectively)<br>• Primary TV was best predictor of recurrence (HR 4.7, $p = 0.001$) and survival (HR 10.0, $p < 0.001$) on multivariate analysis<br>• TV of SCC with locoregional failure was larger compared with those without locoregional failure and those recurring as distant metastases ($p < 0.03$) |
| Kuno et al.[24] | Head and neck SCC (oropharynx, larynx, hypopharynx and oral cavity) | CT texture parameters | Local recurrence after CRT | • 3 histogram features (geometric mean, HR = 4.68, $p = 0.026$; harmonic mean, HR = 8.61, $p = 0.004$; fourth moment, HR = 4.56, $p = 0.048$) and four gray-level run-length features (short-run emphasis, HR = 3.75, $p = 0.044$; gray-level nonuniformity, HR = 5.72, $p = 0.004$; run-length nonuniformity, HR 4.15, $p = 0.043$; short-run low gray-level emphasis, HR = 5.94, $p = 0.035$) were significant predictors of outcome after adjusting for clinical variables |
| Feliciani et al.[25] | Head and neck SCC (oral cavity, oropharynx, hypopharynx, nasopharynx and larynx) | Pre-CRT $^{18}$F-FDG PET texture features for prediction of treatment failure | Local control rate, PFS, OS | • Low-intensity long-run emphasis (LILRE) was a significant predictor of outcome regardless of clinical variables (HR <0.001, $p = 0.001$)<br>• Better local failure prediction using multivariate model based on imaging biomarkers than that based on clinical variables alone (c-index 0.76 *vs* 0.65) |
| Holzapfel et al.[26] | SCC cervical nodal metastases | ADC | Diagnostic accuracy for differentiating between benign and metastatic lymph nodes | • ADC values of malignant lymph nodes were significantly lower than ADC values of benign lymph nodes ($0.78 \pm 0.09$ vs $1.24 \pm 0.16\times10^{-3}$ $mm^2/s$, $p < 0.05$)<br>• 94.3% of lesions were correctly classified as benign or malignant using a threshold ADC value of $1.02 \times 10^{-3}$ $mm^2/s$ (AUC 0.975) |
| Jin et al.[27] | Nasopharyngeal SCC cervical nodal metastases* | ADC | Diagnostic accuracy for differentiating between benign and metastatic lymph nodes | • Benign lymph nodes had higher ADC values than metastatic nodes ($1.110 \pm 0.202$ vs $0.878 \pm 0.159\times10^{-3}$ $mm^2/s$, $p < 0.05$)<br>• An ADC cut-off value of $0.924 \times 10^{-3}$ $mm^2/s$ yielded a sensitivity, specificity, PPV, NPV and accuracy of 83.56%, 82.74%, 80.79%, 85.28%, and 82.80%, respectively for differentiating metastatic from benign lymph nodes (AUC 0.851) |

(Continued)

Table 1. (Continued)

| Reference | Tumour type and location | Imaging features | Endpoints | Main findings |
|---|---|---|---|---|
| Hwang et al.[28] | Head and neck SCC (oral cavity, oropharynx, sinonasal cavity, nasopharynx, hypopharynx, external auditory canal) | ADC | Diagnostic accuracy for differentiating tumour recurrence from post-treatment (surgery and/or chemo/radiotherapy) changes | • Significantly lower $ADC_{1000}$ in recurrent tumour than in post-treatment changes ($p < 0.001$)<br>• Significantly higher $ADC_{ratio}$ in recurrent tumour than that in post-treatment changes (73.5 ±7.2% vs 56.9 ±8.8%, $p < 0.001$)<br>• $ADC_{ratio}$ was the only independently differentiating variable ($p = 0.024$)<br>• An $ADC_{ratio}$ cut-off value of 62.6% yielded a sensitivity, specificity and accuracy of 95.0%, 69.2% and 84.8%, respectively |
| Ryoo et al.[29] | Head and neck SCC (oral cavity, oropharynx, nasopharynx, supraglottic larynx, maxillary sinus) | ADC | Diagnostic accuracy for predicting response to induction chemotherapy | • Good responders had significantly lower $ADC_{2000}$ values than poor responders ($0.62 \pm 0.14$ vs $0.76 \pm 0.15 \times 10^{-3}$ mm²/s, $p = 0.02$)<br>• Mean $ADC_{2000}$ was a significant predictor of response to induction chemotherapy at multiple logistic regression analysis ($p = 0.04$) |
| Preda et al.[30] | Head and neck SCC | SUV, ADC | DFS | • Patients with $SUV_{maxT/B} \geq 5.75$ had an overall worse prognosis ($p = 0.003$)<br>• Lymph node status- and diameter-adjusted $SUV_{maxT/B}$ and $ADC_{min}$ were significant predictors of DFS (HR = 10.37 and 3.26 for $SUV_{maxT/B} \geq 5.75$ and $ADC_{min} \geq 0.58 \times 10^{-3}$ mm²/s, respectively)<br>• In patients with $SUV_{maxT/B} \geq 5.75$, high $ADC_{min}$ was a significant predictor of worse prognosis (adjusted HR = 3.11) |
| Surov et al.[31] | Head and neck SCC | SUV, ADC | Tumour proliferation indexes (Ki67, cell count, total nucleic area, average nucleic area) | • $ADC_{mean}$ correlated with Ki67 level ($r = -0.728$, $p = 0.011$) and total nucleic area ($r = -0.691$, $p = 0.019$)<br>• $ADC_{max}$ correlated with Ki67 level ($r = -0.633$, $p = 0.036$)<br>• Combined parameter $SUV_{max}/ADC_{min}$ correlated with average nucleic area ($r = 0.627$, $p = 0.039$) |
| Dong et al.[34] | Head and neck SCC | DCE-MRI ($K_{trans}$, $V_e$, iAUC) | Tumour grading | • Higher $K_{trans}$, $V_e$ and iAUC in poorly differentiated than in well differentiated SCC ($p < 0.001$, 0.013 and <0.001, respectively)<br>• $K_{trans}$ had the greatest diagnostic significance, with a cut-off value of 0.270 $min^{-1}$ yielding a Youden index, sensitivity and specificity of 0.859, 95.0% and 90.9%, respectively |
| Chen et al.[35] | Head and neck cancer (nasopharynx, oropharynx, tongue base, larynx) | DCE-MRI ($K_{trans}$, $V_e$, $k_{ep}$) | Differentiation among tumours, metastatic nodes and normal tissue | • $K_{trans}$ and $V_e$ of normal tissue ($0.159 \pm 0.087$ $min^{-1}$ and $0.229 \pm 0.146$) were lower than those of nodes ($0.332 \pm 0.149$ $min^{-1}$ and $0.408 \pm 0.124$, $p < 0.001$) and primary tumours ($0.251 \pm 0.066$ $min^{-1}$ and $0.344 \pm 0.081$, $p < 0.001$), respectively<br>• $k_{ep}$ values of primary tumours ($0.621 \pm 0.195$ $min^{-1}$) were significantly higher than those of nodes ($0.429 \pm 0.206$ $min^{-1}$, $p = 0.001$) and normal tissue ($0.420 \pm 0.170$ $min^{-1}$, $p = 0.002$) |

(Continued)

Table 1. (Continued)

| Reference | Tumour type and location | Imaging features | Endpoints | Main findings |
|---|---|---|---|---|
| Baker et al.[36] | Head and neck SCC murine xenografts | R1 and R2* relaxation, functional MRI, relative $^{18}$F-FDG uptake | Association with acquired resistance to targeted EGFR therapy within size-matched EGFR TKI-resistant CAL 27 ($CAL^R$) and sensitive ($CAL^S$) tumour xenografts *in vivo* | • Lower baseline R2* (58 ± 2 vs 70 ± 2 $s^{-1}$), hyperoxia-induced ΔR2* (−4 ± 1 vs −11 ± 2 $s^{-1}$) and volume transfer constant $K_{trans}$ values in $CAL^R$ than in $CAL^S$ tumours ($p < 0.01$), associated with significantly lower Hoechst 33342 uptake and greater pimonidazole-adduct formation<br>• Higher relative $^{18}$F-FDG uptake in the $CAL^R$ cohort (48%, $p < 0.05$), associated with significantly greater Glut-1 expression |
| Zhong et al.[37] | Lymph node metastases from head and neck SCC (larynx, tongue, nasopharynx, floor of mouth, nasal cavity, oropharynx, gingiva) | Preoperative DWI and perfusion CT | Diagnostic accuracy for differentiation between metastatic and benign lymph nodes | • Lower mean ADC in metastatic than in benign nodes (0.849 ± 0.111 vs 1.443 ± 0.406×$10^{-3}$ $mm^2/s$, $p = 0.011$)<br>• Higher BF (114.62 ± 14.26 vs 67.82 ± 13.84 ml/100 g/min, $p = 0.002$) and lower MTT (5.56 ± 0.39 vs 9.46 ± 3.23 s, $p = 0.002$) in metastatic than in benign nodes<br>• An ADC cut-off value of 0.960 × $10^{-3}$ $mm^2/s$ yielded a sensitivity, specificity, PPV, NPV and diagnostic accuracy of 89.58%, 76.47%, 91.48%, 72.22% and 86.15%, respectively<br>• ADC had better diagnostic accuracy than perfusion CT in differentiating metastatic from benign lymph nodes (AUC 0.320 *vs* 0.605, $p < 0.001$) |
| Lam et al.[40] | Head and neck SCC (primary and lymph node metastases) | DECT image quality | SNR, attenuation difference between tumour and muscles, lesion CNR | • 65keV monochromatic images yielded optimal signal-to-noise ratio for all tissues ($p < 0.0001$)<br>• 40keV monochromatic images yielded best tumour attenuation ($p < 0.0001$), attenuation difference between tumour and muscles ($p = 0.03$), and lesion CNR ($p < 0.0001$) |
| Tawfik et al.[43] | Metastatic SCC cervical lymph nodes | DECT-derived iodine content and iodine overlay | Differentiation among normal, inflammatory and metastatic SCC lymph nodes | • Iodine content was significantly lower for metastatic lymph nodes (2.34 ± 0.45 mg $ml^{-1}$) than for normal (2.86 ± 0.37 mg $ml^{-1}$) and inflammatory (3.53 ± 0.56 mg $ml^{-1}$) lymph nodes ($p < 0.0001$)<br>• An iodine content cut-off <2.85 mg $ml^{-1}$ to diagnose nodal metastases had 85% sensitivity and 87.5% specificity (AUC 0.923)<br>• Iodine overlay was significantly lower for metastatic lymph nodes (47 ± 11.6 HU) than normal (57.4 ± 8.2 HU) and inflammatory nodes (69.3 ± 11.5 HU) ($p < 0.0001$)<br>• An iodine overlay cut-off <57.5 HU to diagnose nodal metastases had 90% sensitivity and 78% specificity (AUC 0.896) |
| Foust et al. 2018[44] | Oropharyngeal SCC with nodal metastases | DECT-derived iodine content and iodine spectral attenuation slope | Diagnostic accuracy for differentiation between metastatic and nonmetastatic lymph nodes | • Iodine content was significantly lower in metastatic than in nonmetastatic nodes (0.96 ± 0.28 vs 1.65 ± 0.38 mg $ml^{-1}$, $p = 0.002$)<br>• Iodine spectral attenuation slope was significantly lower in metastatic than in nonmetastatic nodes (1.33 ± 0.49 vs 1.91 ± 0.64 mg $ml^{-1}$, $p = 0.015$)<br>• A nodal iodine threshold ≤1.3 mg $ml^{-1}$ showed a sensitivity of 84.6% and a specificity of 75.0% (AUC 0.839, $p < 0.0001$)<br>• A nodal spectral attenuation slope threshold ≤1.95 showed a sensitivity of 92.3% and specificity of 50.0% (AUC 0.68, $p = 0.049$) |

(Continued)

Table 1. (Continued)

| Reference | Tumour type and location | Imaging features | Endpoints | Main findings |
|---|---|---|---|---|
| Rizzo et al.[45] | Metastatic lymph nodes from various primary cancers (lung, gynaecological)* | DECT-derived material decomposition maps and intranodal attenuation (HU) distribution | Differentiation between metastatic and nonmetastatic lymph nodes based on spectral structure | • Iodine-fat decomposition values were lower in metastatic than in nonmetastatic lymph nodes (3.50 ± 1.02 vs 4.36 ± 1.06 mg ml$^{-1}$, $p < 0.001$)<br>• Iodine-water decomposition values were lower in metastatic than in nonmetastatic lymph nodes (22.4 ± 9.0 vs 31.6 ± 9.8×100 μg ml$^{-1}$, $p < 0.001$)<br>• HU distribution showed a significant gradient from centre to periphery within non-metastatic lymph nodes (up to 20–30% from the centre at 40keV, $p < 0.035$)<br>• Metastatic lymph nodes showed no significant HU gradient |

ADC, apparent diffusion coefficient; AUC, area under the ROC curve; CNR, contrast-to-noise ratio; DFS, disease free survival; HR, hazard ratio; NPV, negative predictive value; OS, overall survival; PFS, progression free survival; PPV, positive predictive value; SNR, signal-to-noise ratio; SUV, standardised uptake value.
[a]Meta-analysis article. (*) References 27 and 45 were included due to the general value of their respective findings, although not specific to oropharyngeal cancer.

Similarly, perfusion CT can quantify the vascularity of primary head-and-neck SCC by applying specific bio-mathematical models of tumour neoangiogenesis (Figure 1). Evidence exists that a) better treatment response can be usually be predicted at perfusion CT before the beginning of therapy in more perfused tumours, and b) early perfusion response to CRT can be assessed before the onset of morphological changes at conventional morphological imaging.[37,38] On the other hand, DECT is emerging as an increasingly widespread imaging technique that can join the fast imaging time, high spatial resolution, and excellent morphological detail of multidetector CT with the possibility to collect functional data via material decomposition, allowing to calculate iodine content as a biomarker of tumour vascularity with a potentially lower overall radiation and contrast dose compared with standard single-energy CT imaging[39] (Figure 2). DECT can be effective in improving the detection and local staging of primary tumours, with particular reference to N-staging, which is often limited due to small and/or morphologically indeterminate lymph nodes leading to inconclusive findings at conventional anatomical imaging.[38,40–42] To this regard, Tawfik et al reported significant differences in DECT-derived iodine content and overlay among normal, inflammatory and metastatic SCC lymph nodes.[43] Moreover, DECT showed lower iodine content and spectral attenuation slope in metastatic oropharyngeal SCC than in non-neoplastic cervical lymph nodes, in line with the finding of a different intranodal iodine distribution that reflects pathological structure.[44,45]

Overall, the integration of quantitative image biomarkers in the diagnostic workup of patients with oropharyngeal cancer and other tumours of the uppermost portion of the digestive tract looks promising in an effort to optimise lesion detection and staging, either at primary sites (especially in case of suspected disease recurrence, when diagnosis by conventional imaging is often hampered by gross post-treatment sequelae) and at lymph node levels (possibly overcoming the poor performance of standard morphological imaging in differentiating smaller benign from metastatic lymph nodes and guiding the choice towards more or less aggressive lymph node resection). Moreover, the correlation between imaging biomarkers and the biological features of tumours (related *e.g.* to lesion aggressiveness) may be of great value to improve patient selection for the best possible treatment in an individualised fashion.

## OESOPHAGEAL AND GASTRIC CANCER

Oesophageal cancer is the eighth most common cancer and the sixth most common cause of cancer-related deaths worldwide, accounting for more than 509,000 deaths in 2018.[46] While initial staging of oesophago-gastric cancer is usually performed with contrast-enhanced CT, multimodality imaging with endoscopic ultrasound and $^{18}$F-FDG PET is useful to define local disease extent and rule out metastatic spread in patients being considered for curative treatment, in an effort to reduce futile surgery.[47] MRI is a less routinely used, yet valuable tool that can reveal the detailed anatomic structure of the oesophagus, differentiating among the various wall layers for proper local staging and providing an accurate assessment of lesion length before and after radiation therapy.[48,49]

Figure 1. An 83-year-old male with locally advanced, partially necrotic gingival SCC as displayed on standard morphological CT image (a). Quantitative CT perfusion analysis revealed increased blood flow (BF) (b), blood volume (BV) (c), permeability surface (PS) product (d), and reduced mean transit time (MTT) (e) values in the viable portion of the tumour compared with contralateral normal tissue (Ref) taken as reference. Note lack of perfusion inside the necrotic portion of the tumour as visually depicted on colour-coded perfusion maps.

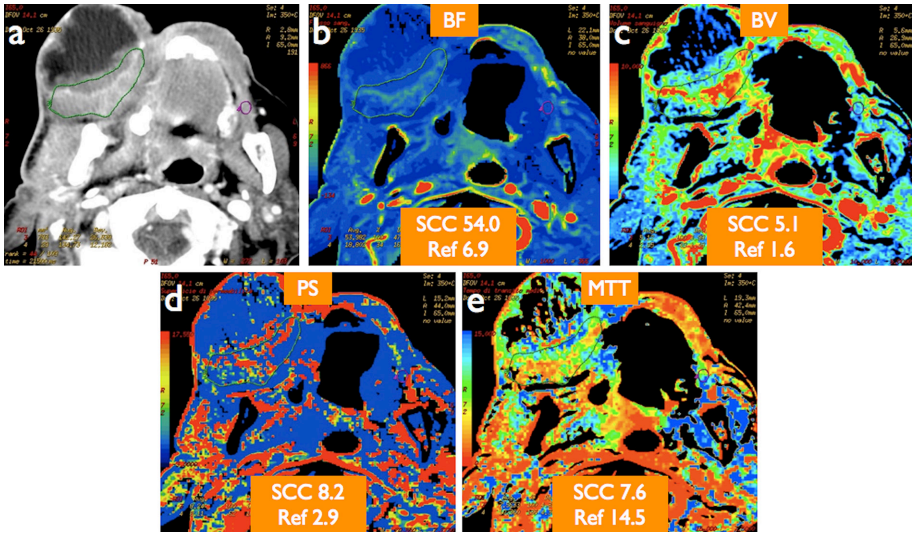


Figure 2. A 51-year-old female with small keratinising SCC of the left retromolar trigone (arrow on DECT monochromatic 55keV image, (a). Material decomposition iodine/water image (b) improves lesion conspicuity by boosting iodine signal and reveals high lesion vascularisation (measured mean iodine concentration of 32 × 100 μg ml$^{-1}$), whereas virtual precontrast image (c) shows no abnormal density or beam hardening artefacts at the lesion site. Avid lesion enhancement was confirmed by spectral curve analysis (d). All images had been obtained at the same anatomic level from a single contrast-enhanced DECT acquisition.

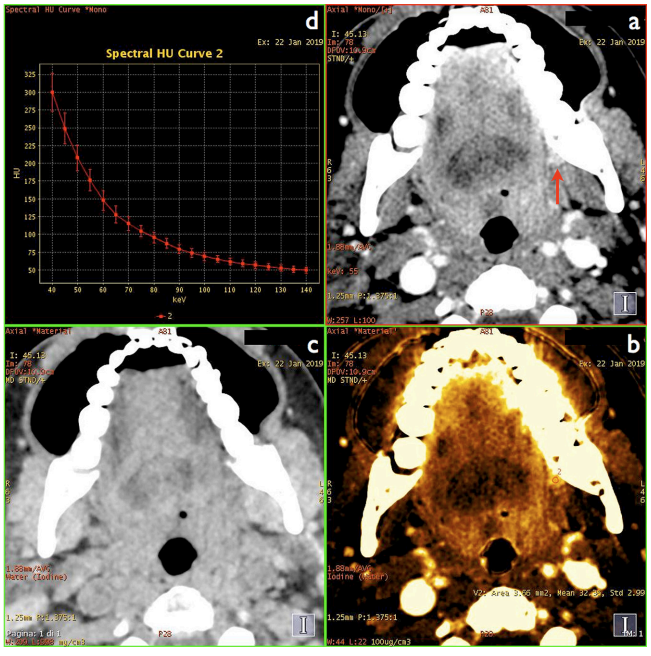


Several imaging biomarkers have been identified that can help predict response of oesophageal cancer to CRT (Table 2). In this latter setting, Aoyagi et al reported that ADC values were significantly higher in patients with better survival rates,[50] whereas in a recent meta-analysis the variation of ADC before and after treatment and post-treatment ADC were found to have good performance for evaluating CRT response.[51] Furthermore, van Rossum et al showed that a treatment-induced relative increase in ADC during the first 2–3 weeks of neoadjuvant CRT for oesophageal cancer was highly predictive of histopathologic response,[52] and also AUC changes at DCE-MRI were predictive of complete pathological response to neoadjuvant CRT at a threshold of −24.6% with sensitivity, specificity, positive and negative predictive values of 83%, 88%, 71% and 93%, respectively.[53]

In parallel, a comparative study of DECT and standardised iodine concentrations in patients with oesophageal cancer before and after CRT showed a significant reduction of tumour normalised iodine concentration on iodine maps in responders, allowing to functionally evaluate treatment response and prognosis in terms of reduced tumour iodine uptake.[46] Radiomics approaches have also recently been proposed for preoperative prediction of lymph node metastasis[54] and tumour response to CRT in patients with oesophageal cancer,[55,56] and of note, it has emerged that radiomics features can outperform size criteria in discriminating lymph node metastasis in resectable oesophageal SCC.[57]

Gastric cancer is the fourth most common malignancy and the second most common cause of cancer-related death worldwide (738,000 deaths annually), whose prognosis and survival rate are poor in advanced stage disease and for which only

Table 2. Summary of the features and main findings of the studies on imaging biomarkers in oesophageal cancer cited in the text. Case reports and general reviews articles are not included. References are sorted in the order in which they appear in the text

| Reference | Tumour type and location | Imaging features | Endpoints | Main findings |
|---|---|---|---|---|
| Ge et al.[46] | Oesophageal cancer | Pre- and post-CRT DECT-derived normalised iodine concentration (NIC) and normalised CT (NCT) values | Comparison of pre- and post-CRT NIC and NCT values obtained in the arterial (NIC-A, NCT-A) and portal venous phases (NIC-V, NCT-V) in good and poor responders | • Post-CRT NIC-A, NIC-V, NCT-A and NCT-V values were significantly lower than before CRT in good responders (0.23 ± 0.05 vs 0.28 ± 0.05, 0.49 ± 0.06 vs 0.54 ± 0.06, 0.27 ± 0.04 vs 0.34 ± 0.06, 0.50 ± 0.04 vs 0.57 ± 0.80, respectively; $p < 0.05$)<br>• Post-CRT NIC-A, NIC-V, NCT-A and NCT-V values were significantly lower in good than in poor responders (0.23 ± 0.05 vs 0.29 ± 0.06, 0.49 ± 0.06 vs 0.51 ± 0.06, 0.27 ± 0.04 vs 0.31 ± 0.04, 0.50 ± 0.04 vs 0.54 ± 0.05, respectively; $p < 0.05$)<br>• Post-CRT NIC-V and NCT-V values in poor responders were significantly lower than before CRT (0.51 ± 0.06 vs 0.56 ± 0.06 and 0.54 ± 0.05 vs 0.59 ± 0.04, respectively; $p < 0.05$) |
| Guo et al.[49] | Oesophageal cancer (SCC, adenocarcinoma, small cell carcinoma) | CT, ADC | Diagnostic accuracy before treatment, outcome prediction during and after radiotherapy in CR and PR patients | • Significantly greater difference in length of oesophageal lesions measured at CT (1.15 ± 0.59 cm) than at DWI (from 0.19 ± 0.36 cm at $b = 600$ mm$^2$/s to 0.84 ± 0.53 cm at $b = 1000$ mm$^2$/s) compared with pathological specimens ($p < 0.05$)<br>• Higher diagnostic rate at DWI than at CT (98.72% *vs* 88.46%, $p = 0.022$)<br>• After radiotherapy, the clinical control rate and 3-year survival rate in the high ADC value group were higher than in the low ADC value group (90.24% *vs* 67.57%, $p = 0.028$ and 58.54% *vs* 32.43%, $p = 0.037$, respectively)<br>• In the second week during radiotherapy and at the end of radiotherapy, the ADC values in the CR group were significantly higher than in the PR group ($p < 0.05$)<br>• ADC values measured in the second week during radiotherapy and at the end of radiotherapy had an AUC of 0.776 and 0.935, respectively for predicting the CR rate of radiotherapy |
| Aoyagi et al.[50] | Oesophageal SCC | Pre-CRT ADC | Prediction of CRT response or prognosis | • Higher ADC values were associated with CRT response (1.27 ± 0.17 vs 0.92 ± 0.28×10$^{-3}$ mm$^2$/s, $p < 0.01$)<br>• ADC values higher than the average ADC of oesophageal cancer tissue (1.10 × 10$^{-3}$ mm$^2$/s) were associated with a higher survival rate (median OS according to ADC of 309 *vs* 197 days, $p = 0.02$) |
| Cheng et al.[51] | Oesophageal cancer | ADC [ADC variation before and after CRT (ΔADC), post-ADC] | Prediction of early response to CRT | • ΔADC showed a pooled sensitivity, specificity, diagnostic odds ratio, and AUC of 93%, 85%, 78 and 0.91<br>• Post-ADC showed a pooled sensitivity, specificity, diagnostic odds ratio, and AUC of 75%, 90%, 26 and 0.85 |
| van Rossum et al.[52] | Oesophageal cancer (adenocarcinoma, SCC) | ADC [ADC variation during treatment ($\Delta ADC_{during}$)] | Prediction of pathologic response to neoadjuvant CRT | • $\Delta ADC_{during}$ was significantly higher in patients with *vs* without pathologic CR (34.6±10.7% vs 14.0±13.1%, $p = 0.016$) and in good *vs* poor responders (30.5±8.3% vs 9.5±12.5%, $p = 0.002$)<br>• $\Delta ADC_{during}$ was predictive of residual cancer at a threshold of 29% (sensitivity, specificity, PPV and NPV of 100%, 75%, 94% and 100%, respectively)<br>• $\Delta ADC_{during}$ was predictive of poor pathologic response at a threshold of 21% (sensitivity, specificity, PPV and NPV of 82%, 100%, 100% and 80%, respectively) |

(Continued)

Table 2. (Continued)

| Reference | Tumour type and location | Imaging features | Endpoints | Main findings |
|---|---|---|---|---|
| Heethuis et al.[53] | Oesophageal cancer (SCC, adenocarcinoma, adenosquamous carcinoma) | DCE-MRI [change of AUC before neoadjuvant CRT (AUCpre), at 2–3 weeks during neoadjuvant CRT (AUCper), and after neoadjuvant CRT before surgery (AUCpost)] | Prediction of pathologic response to neoadjuvant CRT | • The difference between AUCper and AUCpre was most predictive for good response at a threshold of 22.7% (sensitivity, specificity, PPV and NPV of 92%, 77%, 79% and 91%, respectively)<br>• The difference between AUCpost and AUCpre was most predictive for pathologic complete response at a threshold of −24.6% (sensitivity, specificity, PPV and NPV of 83%, 88%, 71% and 93%, respectively) |
| Shen et al.[54] | Lymph node metastases from oesophageal cancer | CT radiomics features | Prediction of lymph node metastasis status in the preoperative setting | • Significant association between radiomics signature and lymph node metastasis ($p < 0.001$), with an AUC of 0.806 and 0.771 in the training and validation cohort, respectively<br>• Good discrimination of the predictive nomogram model (Harrell's Concordance Index of 0.768 and 0.754 in the training and validation cohort, respectively) |
| Hou et al.[55] | Oesophageal carcinoma | CT radiomics features | Prediction of CRT response | • Five radiomics features (Histogram2D_skewness, Histogram2D_kurtosis, GLSZM2D_LZE, Gabor2D_MSA-54, Gabor2D_MSE-54) discriminated nonresponders from responders (AUCs 0.686÷0.727)<br>• Two features (Histogram2D_skewness and Histogram2D_kurtosis) allowed differentiating SDs from PRs ($p = 0.015$ and $p = 0.039$, respectively)<br>• One feature (Histogram2D_skewness) allowed differentiating SDs from CRs ($p = 0.027$)<br>• Both ANN and SVM models had high accuracy for potentially predicting treatment response (ANN 0.972, SVM 0.891) |
| Hou et al.[56] | Oesophageal SCC | MRI radiomics features (T2w, SPAIR T2w) | Prediction of CRT response | • CRs *vs* SDs, PRs *vs* SDs, and responders (CRs and PRs) *vs* nonresponders (SDs) could be differentiated by 26, 17, and 33 features (T2w: 11/11/15, SPAIR T2w: 15/6/18), respectively<br>• Prediction models (ANN and SVM) based on features extracted from SPAIR T2w sequences showed higher accuracy than those derived from T2w sequences (SVM 0.929 *vs* 0.893 and ANN 0.883 *vs* 0.861, respectively) |
| Tan et al.[57] | Lymph node metastases from resectable oesophageal SCC | CT radiomics features | Diagnostic accuracy | • The radiomics signature including five features was significantly associated with lymph node metastasis<br>• The radiomics nomogram [incorporating the signature and CT-reported lymph node status (*i.e.* size criteria)] distinguished lymph node metastasis with an AUC of 0.758 and 0.773 in the training and test set, respectively<br>• Discrimination of the radiomics nomogram exceeded that of size criteria alone in both the training ($p < 0.001$) and test sets ($p = 0.005$)<br>• Integrated discrimination improvement (IDI) and categorical net reclassification improvement (NRI) showed significant improvement in prognostic value when the radiomics signature was added to size criteria in the test set (IDI 17.3%, $p < 0.001$; categorical NRI 52.3%, $p < 0.001$) |

CR, complete response; PR, partial response; SD, stable disease.

Table 3. Summary of the features and main findings of the studies on imaging biomarkers in gastric cancer cited in the text. Case reports and general reviews articles are not included. References are sorted in the order in which they appear in the text

| Reference | Tumour type and location | Imaging features | Endpoints | Main findings |
|---|---|---|---|---|
| Giganti et al.[58] | Resectable gastric cancer (adenocarcinoma, signet-ring cell carcinoma) | ADC | Association between ADC and clinicopathological factors (*i.e.* pathologic T and N stages, tumour location, surgical approach, histologic subtype) | • ADC values ≤ $1.5\times10^{-3}$ $mm^2$/sec were associated with a negative prognosis in the total population (log-relative risk 1.73, standard error 0.56, $p = 0.002$) and in the surgery-only (log-relative risk 1.97, standard error 0.66, $p = 0.003$) and chemotherapy (log-relative risk 2.93, standard error 1.41 $p = 0.03$) groups<br>• ADC values ≤ $1.5\times10^{-3}$ $mm^2$/sec were associated with other significant prognostic factors, especially pathologic T and N stages ($p < 0.001$ and $p < 0.017$, respectively) |
| Liu et al.[61] | Gastric cancer (tubular or papillary adenocarcinoma, poorly cohesive adenocarcinoma, signet-ring cell carcinoma) | CT texture parameters in the arterial (AP) and portal venous phase (PVP) | Diagnostic accuracy and correlation between preoperative CT texture parameters and pathological stage | • Maximum frequency in the AP and mean, maximum frequency, mode in the PVP correlated positively with T stage, N stage, and overall stage (all $p < 0.05$)<br>• Entropy in the PVP correlated positively with N stage ($p = 0.009$) and overall stage ($p = 0.032$)<br>• Skewness in the AP had the highest AUC (0.822) in identifying early from advanced gastric cancers<br>• At multivariate analysis four parameters (maximum frequency, skewness, entropy in the PVP, and differentiation degree from biopsy) allowed prediction of lymph node metastasis, distinguishing gastric cancers with and without lymph node metastasis with an AUC of 0.892 |
| Liu et al.[62] | Gastric cancer (tubular adenocarcinoma, papillary adenocarcinoma, poorly cohesive adenocarcinoma, signet-ring cell carcinoma, mucinous carcinoma, mixed types) | CT texture parameters | Prediction of histopathological characteristics | • Mean attenuation, maximum attenuation, all percentiles and mode derived from PVP images correlated significantly with differentiation degree and Lauren classification ($r = -0.231 \sim -0.324$, $0.228 \sim 0.321$, respectively; $p < 0.05$)<br>• Standard deviation and entropy derived from AP images correlated significantly with Lauren classification ($r = -0.265, -0.222$, respectively; $p < 0.05$)<br>• Standard deviation and entropy on AP images were significantly lower in cancers with than without vascular invasion ($p = 0.035$ and $p = 0.031$, respectively)<br>• Minimum attenuation on AP images was significantly higher in cancers with than those without vascular invasion ($p = 0.028$) |
| Liu et al.[63] | Gastric cancer | CT texture parameters | Correlation between CT texture parameters and immunohistochemical markers (E-cadherin, Ki67, VEGFR2 and EGFR) | • Standard deviation, width, entropy, entropy, correlation and contrast from AP and PVP were significantly correlated with E-cadherin expression level (all $p < 0.05$)<br>• The skewness from the AP and the mean and autocorrelation from the PVP were negatively correlated with Ki67 expression level (all $p < 0.05$)<br>• Width, entropy and contrast from the PVP were positively correlated with VEGFR2 expression level (all $p < 0.05$)<br>• CT texture analysis had an AUC of 0.612÷0.715 for predicting E-cadherin, Ki67 and VEGFR2 expression levels |

(Continued)

Table 3. (Continued)

| Reference | Tumour type and location | Imaging features | Endpoints | Main findings |
|---|---|---|---|---|
| Kim et al.[64] | Advanced gastric cancer | CT texture parameters | Prediction of occult peritoneal carcinomatosis (PC) detected at surgery | • Patients with occult PC showed significantly higher average, entropy, standard deviation, and lower correlation ($p < 0.004$ for all)<br>• Entropy was a significant independent predictor for occult PC, with a cut-off value >7.141 applied to the validation cohort yielding 80% sensitivity and 90% specificity for prediction of occult PC |
| Li et al.[65] | Gastric cancer following curative resection | CT radiomics features | Prognosis prediction | • The radiomics nomogram incorporating the radiomics signature and significant clinicopathological risk factors (T stage, N stage, and differentiation) exhibited significant prognostic superiority over clinical nomogram and radiomics signature alone (Harrell concordance index of 0.82 *vs* 0.71 and 0.82 *vs* 0.74, respectively; $p < 0.001$)<br>• Five radiomics features associated with prognosis were correlated with at least one clinicopathological characteristic, including differentiation, tumor size, N stage, TNM stage, and neural invasion (Spearman's rho coefficient 0.26–0.38, $p < 0.05$) |
| Li et al.[66] | Locally advanced gastric cancer | CT radiomics signature | Outcome prediction of neoadjuvant chemotherapy | • One cross-combination machine-learning method derived from AP images had an AUC >0.6<br>• 12 cross-combination machine-learning methods derived from PVP images had an AUC >0.6<br>• A feature selection method based on linear discriminant analysis +random forest classifier achieved a significant prognostic performance for PVP images (AUC 0.722 ± 0.108, accuracy 0.793, sensitivity 0.636, specificity 0.889; $p = 0.041$) |
| Jiang et al.[67] | Gastric adenocarcinoma | CT radiomics signature derived from PVP images | Prediction of survival and response to chemotherapy | • A radiomics signature consisting of 19 selected features was significantly associated with DFS (HR 1.744, $p < 0.0001$) and OS (HR 3.308, $p < 0.0001$) and was as independent prognostic factor<br>• Incorporating the radiomics signature into the radiomics-based nomograms resulted in better performance for the estimation of DFS and OS than TNM staging and clinicopathological nomograms ($p < 0.0001$)<br>• Stage II and III patients with higher radiomics scores exhibited a favorable response to chemotherapy |
| Caivano et al.[68] | Gastric adenocarcinoma | Preoperative ADC | Diagnostic accuracy compared to conventional MRI with pathology as gold standard | • Gastric cancer tissue had lower ADC values than normal gastric walls ($0.811 \pm 0.300$ vs $1.503 \pm 0.430 \times 10^{-3}$ mm$^2$/s, $p < 0.05$)<br>• Metastatic lymph nodes had lower ADC values than nonmetastatic lymph nodes ($1.70 \pm 0.40$ vs $2.10 \pm 0.22 \times 10^{-3}$ mm$^2$/s, $p < 0.05$)<br>• The T factor accuracy of conventional MRI and DWI was 73% and 80%, respectively<br>• The N staging accuracy of conventional MRI and DWI was 80% and 93%, respectively |
| Joo et al.[69] | Gastric cancer | MRI with and without DWI, CT | Diagnostic accuracy for preoperative staging with pathology as gold standard | • For N staging, MRI with DWI demonstrated higher sensitivity, but lower specificity (86.7% and 58.8%, respectively) than MRI without DWI (50.0% and 94.1%) or CT (43.3% and 100%) ($p < 0.05$) |

(Continued)

Table 3. (Continued)

| Reference | Tumour type and location | Imaging features | Endpoints | Main findings |
|---|---|---|---|---|
| He et al.[70] | Gastric cancer | ADC | Correlation between ADC and HER2 expression | • Significant correlation between mean ADC values and HER2 status ($r$ = 0.312, $p$ = 0.037) and scores ($r$ = 0.419, $p$ = 0.004)<br>• Mean ADC values of HER2+ cancers were significantly higher than those of HER2- tumours (1.211 *vs* 0.984 × $10^{-3}$ $mm^2$/s, $p$ = 0.020)<br>• Minimal ADC values of HER2+ cancers were significantly higher than those of HER2- tumours (1.105 *vs* 0.905 × $10^{-3}$ $mm^2$/s, $p$ = 0.036) |
| Zongqiong et al.[71] | Gastric cancer (tubular adenocarcinoma, signet-ring cell carcinoma, mucinous adenocarcinoma) | Perfusion CT | Tumour grading | • BF was higher in poorly and moderately differentiated cancer than in well differentiated cancer (138.59 ± 38.09 and 110.01 ± 31.90 vs 75.28 ± 6.81 ml/100 g/min, $p$ < 0.05)<br>• BV was higher in poorly and moderately differentiated cancer than in well differentiated cancer (21.08 ± 4.11 and 18.18 ± 5.62 vs 9.01 ± 0.94 ml/100g, $p$ < 0.05)<br>• PS was higher in poorly and moderately differentiated cancer than in well differentiated cancer (57.50 ± 13.28 and 40.08 ± 15.82 vs 10.05 ± 0.71 ml/100 g/min, $p$ < 0.05) |
| Zhang et al.[72] | Gastric adenocarcinoma | Perfusion CT | Correlation with histological grading, serosal and lymphatic involvement, distant metastasis, pTNM stage, and microvessel density (MVD) assessed by CD34 immunohistochemical staining | • PS was significantly higher in poorly than in moderately differentiated cancers (16.471 ± 9.003 vs 9.558 ± 5.422 ml/100 g/min, $p$ = 0.04)<br>• PS was significantly correlated with lymphatic involvement (Spearman's rho coefficient 0.480, $p$ = 0.038) and pTNM stage (rho = 0.509, $p$ = 0.026) |
| Liang et al.[73] | Gastric adenocarcinoma | DECT [normalised iodine concentration (NIC) on AP and PVP images] | Correlation with histologic grading, serosal and lymphatic involvement, distant metastasis, pTNM stage and MVD | • Both AP and PVP NIC values were significantly higher in poorly differentiated than in moderately differentiated tumours (0.133 ± 0.032 vs 0.102 ± 0.028, $p$ = 0.005 and 0.419 ± 0.066 vs 0.369 ± 0.044, $p$ = 0.013, respectively)<br>• Significant correlation between NIC and MVD (AP NIC $r$ = 0.423, $p$ = 0.013; PVP NIC $r$ = 0.542, $p$ = 0.001)<br>• Significant difference between the high and low MVD groups with respect to PVP NIC ($p$ = 0.045) |
| Meng et al.[74] | Gastric mucosal cancer | DECT (IC and NIC on AP and PVP images) | Diagnostic accuracy for differentiating gastric cancer from normal gastric mucosa (NGM) and gastric inflammation (GI) | • Mean NIC values of gastric cancer were significantly higher than those of NGM (AP 0.18 ± 0.06 vs 0.12 ± 0.03, PVP 0.62 ± 0.16 vs 0.37 ± 0.08, $p$ < 0.05)<br>• Significantly different IC values in gastric cancer compared with GI and NGM (AP 24.19 ± 8.27, 19.07 ± 5.82 and 13.61 ± 2.52 mg $ml^{-1}$; PVP 28.00 ± 7.01, 24.66 ± 6.5 and 16.94 ± 3.06 mg $ml^{-1}$, respectively; $p$ < 0.05)<br>• NIC and IC in AP had sensitivity of 71.43% and 88.89% in differentiating gastric cancer from NGM<br>• NIC and IC in PVP had sensitivity of 88.89% and 90.48% in differentiating gastric cancer from NGM |

(Continued)

Table 3. (Continued)

| Reference | Tumour type and location | Imaging features | Endpoints | Main findings |
|---|---|---|---|---|
| Pan et al.[75] | Gastric cancer (adenocarcinoma, signet-ring cell carcinoma, mucinous adenocarcinoma) | DECT (keV images, conventional kVp images, NIC) | Diagnostic accuracy with pathology as gold standard | • Overall accuracies for T, N and M staging determined with keV images and conventional kVp images were 81.2%, 80.0%, 98.9% and 73.9%, 75.0%, 98.9%, respectively<br>• Higher accuracy in N-staging using optimal keV images than conventional kVp images (sensitivity, specificity and accuracy of 90.7%, 67.9% and 82.9% *vs* 88.8%, 60.7% and 79.2%; $p < 0.05$)<br>• NIC values were significantly different between differentiated and undifferentiated cancer both in AP (0.21 ± 0.08 vs 0.28 ± 0.16, $p = 0.02$) and PVP (0.54 ± 0.17 vs 0.46 ± 0.12, $p = 0.01$)<br>• NIC values were significantly different between metastatic and nonmetastatic lymph nodes both in AP (0.22 ± 0.09 vs 0.13 ± 0.06, $p < 0.001$) and PVP (0.47 ± 0.14 vs 0.30 ± 0.12, $p < 0.001$)<br>• A threshold value of 0.145 for AP NIC and 0.333 for PVP NIC yielded a sensitivity and specificity of 84.1%, 67.1% and 89.9%, 67.6%, respectively |
| Cheng et al.[76] | Early and advanced gastric adenocarcinoma | DECT [IC, NIC, curve slope ($\lambda_{HU}$) in the PVP and delayed phase (DP)] | Association with Ki-67 protein expression as a marker of cell proliferation | • DECT parameters were significantly lower in early than in advanced gastric cancers both in PVP (IC 19.36 ± 2.82 vs 21.25 ± 4.91 mg ml$^{-1}$; NIC 0.35 ± 0.11 vs 0.42 ± 0.12; $\lambda_{HU}$ 2.20 ± 0.43 vs 2.67 ± 0.63; $p < 0.05$) and DP (IC 16.89 ± 2.07 vs 19.10 ± 4.07 mg ml$^{-1}$; NIC 0.43 ± 0.06 vs 0.58 ± 0.14; $\lambda_{HU}$ 1.99 ± 0.35 vs 2.51 ± 0.64; $p < 0.01$)<br>• DECT parameters were positively correlated with Ki-67 grade (Spearman rho 0.818, 0.753, 0.728 in PVP and 0.730, 0.745, 0.468 in DP, respectively; $p < 0.01$) |

Figure 3. A 49-year-old male with T3N2 advanced gastric cancer without peritoneal seeding showed entropy of 7.05 within the region of interest (a). A 59-year-old female with T3N2 advanced gastric cancer with occult seeding (b) showed entropy of 7.70, higher than the cut-off value (>7.141) obtained from receiver operating characteristic (ROC) curve analysis (c). Reproduced and adapted from.[64]

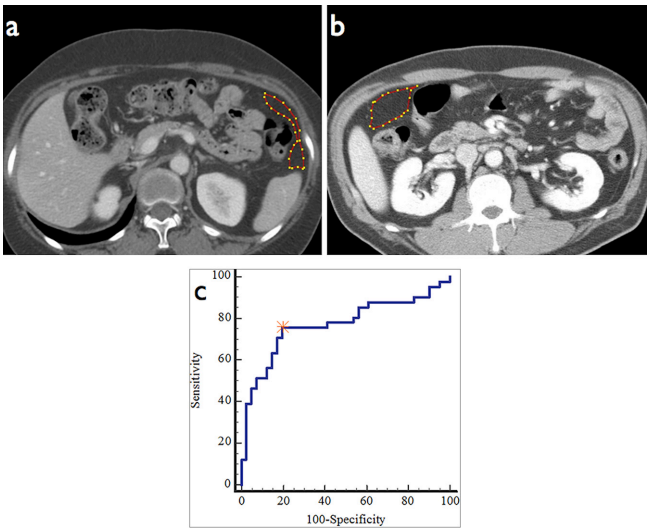


surgical resection of the primary tumour can be curative.[58,59] In light of this, quantitative imaging represents a promising area for gastric cancer research and management, and in particular, ADC and contrast-enhanced CT-based texture features are noninvasive, quantitative imaging biomarkers that hold promise in the evaluation of tumour aggressiveness, treatment response and prognosis (Table 3).[47,60,61] CT texture analysis can predict histopathological characteristics of gastric cancers (such as differentiation degree, Lauren classification and vascular invasion status),[62] the expression level of immunohistochemical biomarkers (including E-cadherin, Ki67, and VEGFR2),[63] and even occult peritoneal carcinomatosis in patients with advanced disease[64] (Figure 3). Radiomic feature extraction is another area of active research that has yielded promising results, especially in terms of prognostic assessment.[47,65–67]

Among quantitative imaging biomarkers, DWI has shown higher accuracy than conventional MRI for T- and N-staging of gastric adenocarcinoma (80% *vs* 73% and 93% *vs* 80%, respectively),[68] and the addition of 3T-MR DWI provides significantly higher sensitivity over conventional MRI or contrast-enhanced CT for the assessment of lymph node metastasis.[69] In a multivariate analysis of 99 patients with gastric cancer (of whom 71 underwent surgery and 28 neoadjuvant chemotherapy, respectively), ADC values of $1.5 \times 10^{-3}$ $mm^2/s$ or lower were associated with a negative prognosis along with pathologic T and N stages, suggesting an important role of DWI in outcome prediction.[58] Overall, such findings seem to reflect a relationship between quantitative imaging biomarkers and different molecular tumour fingerprints that may be exploited to tailor treatment, and to this latter regard it is worth mentioning, for instance, that ADC values were found to correlate with HER2 status.[70]

Perfusion CT and especially DECT can also give a relevant contribution to local staging and prognostic assessment of gastric cancer. Zongqiong et al showed a correlation between perfusion CT parameters (BF, BV and PS values) and the degree of differentiation of gastric adenocarcinoma,[71] whereas Zhang et al reported a significant difference in the PS values between patients with or without lymphatic involvement ($p$ = 0.038), different histological grades ($p$ = 0.04) and TNM staging ($p$ = 0.026).[72] On the other hand, in Liang et al's study DECT-derived normalised iodine content on arterial and portal venous phase acquisitions was higher in poorly differentiated gastric adenocarcinomas than in moderately differentiated tumours, along with a significant difference in portal venous phase normalised iodine content between tumours with high and low microvessel density, as determined by CD34 staining.[73] Quantitative analysis of DECT imaging parameters for the gastric mucosa can be useful to differentiate malignant from benign gastric mucosal lesions, with iodine concentration and normalised iodine concentration in gastric cancer being significantly different from those in normal and inflammatory mucosa, showing a sensitivity and specificity of about 90% in differentiating gastric cancer from normal mucosa on portal venous phase images.[74] More generally, DECT with monochromatic imaging and quantitative iodine concentration measurements has higher diagnostic accuracy than conventional single-energy CT for T and N staging of gastric cancer (81.2% and 80% *vs* 73.9% and 75%, respectively), with iodine concentration indexes differing significantly between differentiated and undifferentiated gastric carcinoma, and between metastatic and non-metastatic lymph nodes.[75] The diagnostic potential of DECT may be pushed even further to a molecular level, with quantitative parameters (such as iodine concentration, normalised iodine concentration, and curve slope) showing a significant positive correlation with Ki-67 antigen expression as a marker of tumour proliferation and allowing to differentiate between early and advanced gastric cancer.[76]

Based on the above considerations, the evidence collected so far shows that imaging biomarkers can provide a significant added value to conventional imaging for improving T and N staging of oesophageal and gastric cancers and predicting early response to neoadjuvant CRT and overall prognosis. This might play a pivotal role into identifying the best treatment strategy for patients on a case-by-case basis [*e.g.* surgery with or without CRT, or neoadjuvant CRT? which degree of surgical radicality? which expected lesion aggressiveness (including conditions with a dramatic impact on treatment choice and prognosis, such as peritoneal dissemination)? any and which potential targets for specific therapies?], possibly leading to better patient outcomes, higher quality of life, and more effective use of healthcare resources.

## CONCLUSIONS

Imaging biomarkers represent an exciting area of active research that can currently be considered a new frontier of oncologic

imaging, owing to their potential to provide a substantial amount of additional information to guide all management steps of cancer patients (from lesion detection and staging to treatment planning, follow-up and prognostic assessment). In particular, the diagnostic workup of upper gastrointestinal cancers should significantly benefit from a combined and thorough analysis of available imaging biomarkers, due to the heterogeneous biological features of such diseases that usually require a complex diagnostic and therapeutic approach. It is likely that in the near future, a growing number of imaging biomarkers and radiomics features will reach the status of validated parameters to be routinely assessed along with established diagnostic imaging criteria, possibly favouring treatment individualisation and improving overall patient outcome.

## REFERENCES


1. Califf RM. Biomarker definitions and their applications. *Exp Biol Med* 2018; **243**: 213–21. doi: https://doi.org/10.1177/1535370217750088
2. FDA-NIH Biomarker Working Group Best (biomarkers, endpoints. *and other Tools) Resource* 2018;Available from.
3. Deigner H. P, Kohl M. eds. *Precision medicine: tools and quantitative approaches*. London, UK: Elsevier; 2018 .
4. European Society of Radiology (ESR). white paper on imaging biomarkers. *Insights Imaging* 2010; **1**: 42–5.
5. Lambin P, Rios-Velazquez E, Leijenaar R, Carvalho S, van Stiphout RGPM, Granton P, et al. Radiomics: extracting more information from medical images using advanced feature analysis. *Eur J Cancer* 2012; **48**: 441–6. doi: https://doi.org/10.1016/j.ejca.2011.11.036
6. Neri E, Regge D. Imaging biobanks in oncology: European perspective. *Future Oncol* 2017; **13**: 433–41. doi: https://doi.org/10.2217/fon-2016-0239
7. Rizzo S, Botta F, Raimondi S, Origgi D, Fanciullo C, Morganti AG, et al. Radiomics: the facts and the challenges of image analysis. *Eur Radiol Exp* 2018; **2**: 36. doi: https://doi.org/10.1186/s41747-018-0068-z
8. Neri E, Del Re M, Paiar F, Erba P, Cocuzza P, Regge D, et al. Radiomics and liquid biopsy in oncology: the holons of systems medicine. *Insights Imaging* 2018; **9**: 915–24. doi: https://doi.org/10.1007/s13244-018-0657-7
9. O'Connor JPB, Aboagye EO, Adams JE, Aerts HJWL, Barrington SF, Beer AJ, et al. Imaging biomarker roadmap for cancer studies. *Nat Rev Clin Oncol* 2017; **14**: 169–86. doi: https://doi.org/10.1038/nrclinonc.2016.162
10. Jansen RW, van Amstel P, Martens RM, Kooi IE, Wesseling P, de Langen AJ, et al. Non-invasive tumor genotyping using radiogenomic biomarkers, a systematic review and oncology-wide pathway analysis. *Oncotarget* 2018; **9**: 20134–55. doi: https://doi.org/10.18632/oncotarget.24893
11. Sala E, Mema E, Himoto Y, Veeraraghavan H, Brenton JD, Snyder A, et al. Unravelling tumour heterogeneity using next-generation imaging: radiomics, radiogenomics, and habitat imaging. *Clinical Radiology* 2017; **72**: 3–10. doi: https://doi.org/10.1016/j.crad.2016.09.013
12. Gillies RJ, Kinahan PE, Hricak H. Radiomics: images are more than pictures, they are data. *Radiology* 2016; **278**: 563–77. doi: https://doi.org/10.1148/radiol.2015151169
13. Global Burden of Disease Cancer Collaboration Global, regional, and National cancer incidence, mortality, years of life lost, years lived with disability-adjusted life-years for 32 cancer groups, 1990 to 2015: a systematic analysis for the global burden of Disease Study. *JAMA Oncol* 2017; **3**: 524–48.
14. Nooij RP, Hof JJ, van Laar PJ, van der Hoorn A. Functional MRI for treatment evaluation in patients with head and neck squamous cell carcinoma: a review of the literature from a radiologist perspective. *Curr Radiol Rep* 2018; **6**: 2. doi: https://doi.org/10.1007/s40134-018-0262-z
15. Talebi Ghane E, Baghestani AR, Zayeri F, Talimkhani I, Masoudi S. Survival and recurrence rate in patients with head and neck cancer and associated prognostic factors. *Int J Cancer Manag* 2018; **11**: e12794.
16. Windon MJ, D'Souza G, Fakhry C. Treatment preferences in human papillomavirus-associated oropharyngeal cancer. *Future Oncol* 2018; **14**: 2521–30. doi: https://doi.org/10.2217/fon-2018-0063
17. Oksuz DC, Prestwich RJ, Carey B, Wilson S, Senocak MS, Choudhury A, et al. Recurrence patterns of locally advanced head and neck squamous cell carcinoma after 3D conformal (chemo)-radiotherapy. *Radiat Oncol* 2011; **6**: 54. doi: https://doi.org/10.1186/1748-717X-6-54
18. Saito N, Nadgir RN, Nakahira M, Takahashi M, Uchino A, Kimura F, et al. Posttreatment CT and MR imaging in head and neck cancer: what the radiologist needs to know. *Radiographics* 2012; **32**: 1261–82. doi: https://doi.org/10.1148/rg.325115160
19. Lewis-Jones H, Colley S, Gibson D. Imaging in head and neck cancer: United Kingdom National multidisciplinary guidelines. *J Laryngol Otol* 2016; **130**(S2): S28–S31. doi: https://doi.org/10.1017/S0022215116000396
20. van der Hoorn A, van Laar PJ, Holtman GA, Westerlaan HE. Diagnostic accuracy of magnetic resonance imaging techniques for treatment response evaluation in patients with head and neck tumors, a systematic review and meta-analysis. *PLoS One* 2017; **12**: e0177986: e0177986: . doi: https://doi.org/10.1371/journal.pone.0177986
21. Elhalawani H, Lin TA, Volpe S, Mohamed ASR, White AL, Zafereo J, et al. Machine learning applications in head and neck radiation oncology: lessons from open-source radiomics challenges. *Front Oncol* 2018; **8**: 294. doi: https://doi.org/10.3389/fonc.2018.00294
22. Leijenaar RTH, Bogowicz M, Jochems A, Hoebers FJP, Wesseling FWR, Huang SH, et al. Development and validation of a radiomic signature to predict HPV (p16) status from standard CT imaging: a multicenter study. *Br J Radiol* 2018; **5**: 20170498. doi: https://doi.org/10.1259/bjr.20170498
23. Strongin A, Yovino S, Taylor R, Wolf J, Cullen K, Zimrin A, et al. Primary tumor volume is an important predictor of clinical outcomes among patients with locally advanced squamous cell cancer of the head and neck treated with definitive chemoradiotherapy. *Int J Radiat Oncol Biol Phys* 2012; **82**: 1823–30. doi: https://doi.org/10.1016/j.ijrobp.2010.10.053
24. Kuno H, Qureshi MM, Chapman MN, Li B, Andreu-Arasa VC, Onoue K, et al. CT texture analysis potentially predicts local failure in head and neck squamous cell carcinoma treated with chemoradiotherapy. *AJNR Am J Neuroradiol* 2017; **38**: 2334–40. doi: https://doi.org/10.3174/ajnr.A5407
25. Feliciani G, Fioroni F, Grassi E, Bertolini M, Rosca A, Timon G, et al. Radiomic Profiling of

Head and Neck Cancer: $^{18}$ F-FDG PET Texture Analysis as Predictor of Patient Survival. *Contrast Media Mol Imaging* 2018; **2018**: 1–8. doi: https://doi.org/10.1155/2018/3574310
26. Holzapfel K, Duetsch S, Fauser C, Eiber M, Rummeny EJ, Gaa J. Value of diffusion-weighted MR imaging in the differentiation between benign and malignant cervical lymph nodes. *Eur J Radiol* 2009; **72**: 381–7. doi: https://doi.org/10.1016/j.ejrad.2008.09.034
27. Jin GQ, Yang J, Liu LD, Su DK, Wang DP, Zhao SF, et al. The diagnostic value of 1.5-T diffusion-weighted MR imaging in detecting 5 to 10mm metastatic cervical lymph nodes of nasopharyngeal carcinoma. *Medicine* 2016; **95**: e4286: e4286: . doi: https://doi.org/10.1097/MD.0000000000004286
28. Hwang I, Choi SH, Kim Y-J, Kim KG, Lee AL, Yun TJ, et al. Differentiation of recurrent tumor and posttreatment changes in head and neck squamous cell carcinoma: application of high b-value diffusion-weighted imaging. *AJNR Am J Neuroradiol* 2013; **34**: 2343–8. doi: https://doi.org/10.3174/ajnr.A3603
29. Ryoo I, Kim J-H, Choi SH, Sohn C-H, Kim SC. Squamous Cell Carcinoma of the Head and Neck: Comparison of Diffusion-weighted MRI at b-values of 1,000 and 2,000 s/mm(2) to Predict Response to Induction Chemotherapy. *Magn Reson Med Sci* 2015; **14**: 337–45. doi: https://doi.org/10.2463/mrms.2015-0003
30. Preda L, Conte G, Bonello L, Giannitto C, Travaini LL, Raimondi S, et al. Combining standardized uptake value of FDG-PET and apparent diffusion coefficient of DW-MRI improves risk stratification in head and neck squamous cell carcinoma. *Eur Radiol* 2016; **26**: 4432–41. doi: https://doi.org/10.1007/s00330-016-4284-8
31. Surov A, Stumpp P, Meyer HJ, Gawlitza M, Höhn A-K, Boehm A, et al. Simultaneous (18)F-FDG-PET/MRI: Associations between diffusion, glucose metabolism and histopathological parameters in patients with head and neck squamous cell carcinoma. *Oral Oncol* 2016; **58**: 14–20. doi: https://doi.org/10.1016/j.oraloncology.2016.04.009
32. El Beltagi AH, Elsotouhy AH, Own AM, Abdelfattah W, Nair K, Vattoth S. Functional magnetic resonance imaging of head and neck cancer: performance and potential. *Neuroradiol J* 2018; **6**: 1971400918808546.
33. Jansen JFA, Parra C, Lu Y, Shukla-Dave A. Evaluation of head and neck tumors with functional MR imaging. *Magn Reson Imaging Clin N Am* 2016; **24**: 123–33. doi: https://doi.org/10.1016/j.mric.2015.08.011
34. Dong Ji X, Yan S, Xia S, Guo Y, Shen W. Quantitative parameters correlated well with differentiation of squamous cell carcinoma at head and neck: a study of dynamic contrast-enhanced MRI. *Acta Radiol* 2018; **20**: 284185118809543.
35. Chen L, Ye Y, Chen H, Chen S, Jiang J, Dan G, et al. Dynamic contrast-enhanced magnetic resonance imaging for differentiating between primary tumor, metastatic node and normal tissue in head and neck cancer. *Curr Med Imaging Rev* 2018; **14**: 416–21. doi: https://doi.org/10.2174/1573405614666171205105236
36. Baker LCJ, Sikka A, Price JM, Boult JKR, Lepicard EY, Box G, et al. Evaluating imaging biomarkers of acquired resistance to targeted EGFR therapy in xenograft models of human head and neck squamous cell carcinoma. *Front Oncol* 2018; **8**: 271. doi: https://doi.org/10.3389/fonc.2018.00271
37. Faggioni L, Neri E, Bartolozzi C. CT perfusion of head and neck tumors: how we do it. *AJR Am J Roentgenol* 2010; **194**: 62–9. doi: https://doi.org/10.2214/AJR.09.3187
38. Zhong J, Lu Z, Xu L, Dong L, Qiao H, Hua R, et al. The diagnostic value of cervical lymph node metastasis in head and neck squamous carcinoma by using diffusion-weighted magnetic resonance imaging and computed tomography perfusion. *Biomed Res Int* 2014; **2014**: 1–7. doi: https://doi.org/10.1155/2014/260859
39. Parakh A, Macri F, Sahani D. Dual-energy computed tomography: dose reduction, series reduction, and contrast load reduction in dual-energy computed tomography. *Radiol Clin North Am* 2018; **56**: 601–24. doi: https://doi.org/10.1016/j.rcl.2018.03.002
40. Forghani R, De Man B, Gupta R. Dual-energy computed tomography: physical principles, approaches to scanning, usage, and implementation: Part 1. *Neuroimaging Clin N Am* 2017; **27**: 371–84. doi: https://doi.org/10.1016/j.nic.2017.03.002
41. Pérez-Lara A, Forghani R. Spectral computed tomography: technique and applications for head and neck cancer. *Magn Reson Imaging Clin N Am* 2018; **26**: 1–17. doi: https://doi.org/10.1016/j.mric.2017.08.001
42. Lam S, Gupta R, Levental M, Yu E, Curtin HD, Forghani R. Optimal virtual monochromatic images for evaluation of normal tissues and head and neck cancer using dual-energy CT. *AJNR Am J Neuroradiol* 2015; **36**: 1518–24. doi: https://doi.org/10.3174/ajnr.A4314
43. Tawfik AM, Razek AA, Kerl JM, Nour-Eldin NE, Bauer R, Vogl TJ. Comparison of dual-energy CT-derived iodine content and iodine overlay of normal, inflammatory and metastatic squamous cell carcinoma cervical lymph nodes. *Eur Radiol* 2014; **24**: 574–80. doi: https://doi.org/10.1007/s00330-013-3035-3
44. Foust AM, Ali RM, Nguyen XV, Agrawal A, Prevedello LM, Bourekas EC, et al. Dual-energy CT-derived iodine content and spectral attenuation analysis of metastatic versus nonmetastatic lymph nodes in squamous cell carcinoma of the oropharynx. *Tomography* 2018; **4**: 66–71. doi: https://doi.org/10.18383/j.tom.2018.00009
45. Rizzo S, Radice D, Femia M, De Marco P, Origgi D, Preda L, et al. Metastatic and non-metastatic lymph nodes: quantification and different distribution of iodine uptake assessed by dual-energy CT. *Eur Radiol* 2018; **28**: 760–9. doi: https://doi.org/10.1007/s00330-017-5015-5
46. Ge X, Yu J, Wang Z, Xu Y, Pan C, Jiang L, et al. Comparative study of dual energy CT iodine imaging and standardized concentrations before and after chemoradiotherapy for esophageal cancer. *BMC Cancer* 2018; **18**: 1120. doi: https://doi.org/10.1186/s12885-018-5058-2
47. Sah B-R, Owczarczyk K, Siddique M, Cook GJR, Goh V. Radiomics in esophageal and gastric cancer. *Abdom Radiol* 2018; **24**. doi: https://doi.org/10.1007/s00261-018-1724-8
48. Tomizawa M, Shinozaki F, Ozaki A, Baba A, Fukamizu Y, Matsunaga F, et al. Diffusion-weighted imaging and diffusion-weighted whole-body imaging with background body signal suppression for characterizing esophageal cancer: a case report. *Int Med Case Rep J* 2013; **6**: 95–8. doi: https://doi.org/10.2147/IMCRJ.S41823
49. Guo L, Zhang L, Zhao J. CT scan and magnetic resonance diffusion-weighted imaging in the diagnosis and treatment of esophageal cancer. *Oncol Lett* 2018; **16**: 7117–22. doi: https://doi.org/10.3892/ol.2018.9532
50. Aoyagi T, Shuto K, Okazumi S, Shimada H, Kazama T, Matsubara H. Apparent diffusion coefficient values measured by diffusion-weighted imaging predict chemoradiotherapeutic effect for advanced esophageal cancer. *Dig Surg* 2011; **28**: 252–7. doi: https://doi.org/10.1159/000328770
51. Cheng B, Yu J. Predictive value of diffusion-weighted MR imaging in early response to chemoradiotherapy of esophageal cancer: a meta-analysis. *Dis Esophagus* 2018;.
52. van Rossum PSN, van Lier ALHMW, van Vulpen M, Reerink O, Lagendijk JJW, Lin SH, et al. Diffusion-weighted magnetic resonance imaging for the prediction of pathologic response to neoadjuvant chemoradiotherapy in esophageal cancer. *Radiother Oncol* 2015; **115**: 163–70. doi:

https://doi.org/10.1016/j.radonc.2015.04.027

53. Heethuis SE, van Rossum PSN, Lips IM, Goense L, Voncken FE, Reerink O, et al. Dynamic contrast-enhanced MRI for treatment response assessment in patients with oesophageal cancer receiving neoadjuvant chemoradiotherapy. *Radiother Oncol* 2016; **120**: 128–35. doi: https://doi.org/10.1016/j.radonc.2016.05.009
54. Shen C, Liu Z, Wang Z, Guo J, Zhang H, Wang Y, et al. Building CT radiomics based nomogram for preoperative esophageal cancer patients lymph node metastasis prediction. *Transl Oncol* 2018; **11**: 815–24. doi: https://doi.org/10.1016/j.tranon.2018.04.005
55. Hou Z, Ren W, Li S, Liu J, Sun Y, Yan J, Wan S, et al. Radiomic analysis in contrast-enhanced CT: predict treatment response to chemoradiotherapy in esophageal carcinoma. *Oncotarget* 2017; **8**: 104444–54. doi: https://doi.org/10.18632/oncotarget.22304
56. Hou Z, Li S, Ren W, Liu J, Yan J, Wan S. Radiomic analysis in T2W and SPAIR T2W MRI: predict treatment response to chemoradiotherapy in esophageal squamous cell carcinoma. *J Thorac Dis* 2018; **10**: 2256–67. doi: https://doi.org/10.21037/jtd.2018.03.123
57. Tan X, Ma Z, Yan L, Ye W, Liu Z, Liang C. Radiomics nomogram outperforms size criteria in discriminating lymph node metastasis in resectable esophageal squamous cell carcinoma. *Eur Radiol* 2019; **29**: 392–400. doi: https://doi.org/10.1007/s00330-018-5581-1
58. Giganti F, Orsenigo E, Esposito A, Chiari D, Salerno A, Ambrosi A, et al. Prognostic role of diffusion-weighted MR imaging for resectable gastric cancer. *Radiology* 2015; **276**: 444–52. doi: https://doi.org/10.1148/radiol.15141900
59. Sitarz R, Skierucha M, Mielko J, Offerhaus GJA, Maciejewski R, Polkowski WP. Gastric cancer: epidemiology, prevention, classification, and treatment. *Cancer Manag Res* 2018; **10**: 239–48. doi: https://doi.org/10.2147/CMAR.S149619
60. Giganti F, Tang L, Baba H. Gastric cancer and imaging biomarkers: Part 1 – a critical review of DW-MRI and CE-MDCT findings. *Eur Radiol* 2018;.
61. Liu S, Shi H, Ji C, Zheng H, Pan X, Guan W, et al. Preoperative CT texture analysis of gastric cancer: correlations with postoperative TNM staging. *Clinical Radiology* 2018; **73**: 756.e1–756.e9e9. doi: https://doi.org/10.1016/j.crad.2018.03.005
62. Liu S, Liu S, Ji C, Zheng H, Pan X, Zhang Y, et al. Application of CT texture analysis in predicting histopathological characteristics of gastric cancers. *Eur Radiol* 2017; **27**: 4951–9. doi: https://doi.org/10.1007/s00330-017-4881-1
63. Liu S, Shi H, Ji C, Guan W, Chen L, Sun Y, et al. CT textural analysis of gastric cancer: correlations with immunohistochemical biomarkers. *Sci Rep* 2018; **8**: 11844. doi: https://doi.org/10.1038/s41598-018-30352-6
64. Kim HY, Kim YH, Yun G, Chang W, Lee YJ, Kim B. Could texture features from preoperative CT image be used for predicting occult peritoneal carcinomatosis in patients with advanced gastric cancer? *PLoS One* 2018; **13**: e0194755: e0194755: . doi: https://doi.org/10.1371/journal.pone.0194755
65. Li W, Zhang L, Tian C, Song H, Fang M, Hu C, et al. Prognostic value of computed tomography radiomics features in patients with gastric cancer following curative resection. *Eur Radiol* 2018; **1**. doi: https://doi.org/10.1007/s00330-018-5861-9
66. Li Z, Zhang D, Dai Y, Dong J, Wu L, Li Y, et al. Computed tomography-based radiomics for prediction of neoadjuvant chemotherapy outcomes in locally advanced gastric cancer: a pilot study. *Chin J Cancer Res* 2018; **30**: 406–14. doi: https://doi.org/10.21147/j.issn.1000-9604.2018.04.03
67. Jiang Y, Chen C, Xie J, Wang W, Zha X, Lv W, et al. Radiomics signature of computed tomography imaging for prediction of survival and chemotherapeutic benefits in gastric cancer. *EBioMedicine* 2018; **36**: 171–82. doi: https://doi.org/10.1016/j.ebiom.2018.09.007
68. Caivano R, Rabasco P, Lotumolo A, D' Antuono F, Zandolino A, Villonio A, et al. Gastric cancer: the role of diffusion weighted imaging in the preoperative staging. *Cancer Invest* 2014; **32**: 184–90. doi: https://doi.org/10.3109/07357907.2014.896014
69. Joo I, Lee JM, Kim JH, Shin C-I, Han JK, Choi BI. Prospective comparison of 3T MRI with diffusion-weighted imaging and MDCT for the preoperative TNM staging of gastric cancer. *J Magn Reson Imaging* 2015; **41**: 814–21. doi: https://doi.org/10.1002/jmri.24586
70. He J, Shi H, Zhou Z, Chen J, Guan W, Wang H, et al. Correlation between apparent diffusion coefficients and HER2 status in gastric cancers: pilot study. *BMC Cancer* 2015; **15**: 749. doi: https://doi.org/10.1186/s12885-015-1726-7
71. Zongqiong S, Xiaohong L, Wei C, Jiangfeng Z, Yuxi G, Zhihui X, et al. CT perfusion imaging of the stomach: a quantitative analysis according to different degrees of adenocarcinoma cell differentiation. *Clin Imaging* 2016; **40**: 558–62. doi: https://doi.org/10.1016/j.clinimag.2015.11.006
72. Zhang H, Pan Z, Du L, Yan C, Ding B, Song Q, et al. Advanced gastric cancer and perfusion imaging using a multidetector row computed tomography: correlation with prognostic determinants. *Korean J Radiol* 2008; **9**: 119–27. doi: https://doi.org/10.3348/kjr.2008.9.2.119
73. Liang P, Ren X-C, Gao J-B, Chen K-S, Xu X, Ren XC. Iodine concentration in spectral CT: assessment of prognostic determinants in patients with gastric adenocarcinoma. *AJR Am J Roentgenol* 2017; **209**: 1033–8. doi: https://doi.org/10.2214/AJR.16.16895
74. Meng X, Ni C, Shen Y, Hu X, Chen X, Li Z, et al. Differentiating malignant from benign gastric mucosal lesions with quantitative analysis in dual energy spectral computed tomography: initial experience. *Medicine* 2017; **96**: e5878: e5878: . doi: https://doi.org/10.1097/MD.0000000000005878
75. Pan Z, Pang L, Ding B, Yan C, Zhang H, Du L, et al. Gastric cancer staging with dual energy spectral CT imaging. *PLoS One* 2013; **8**: e53651: e53651: . doi: https://doi.org/10.1371/journal.pone.0053651
76. Cheng S-M, Ling W, Zhu J, Xu J-R, Wu L-M, Gong H-X. Dual energy spectral CT imaging in the assessment of gastric cancer and cell proliferation: a preliminary study. *Sci Rep* 2018; **8**: 17619. doi: https://doi.org/10.1038/s41598-018-35712-w